Proceedings of SPIE, Vol. 5089, April 2003

Design and Realization of a Discretely Loaded Resistive Vee Dipole on a Printed Circuit Board

Kangwook Kim and Waymond R. Scott, Jr.

School of Electrical and Computer Engineering
Georgia Institute of Technology
Atlanta, Georgia 30332-0250

ABSTRACT

A discretely loaded resistive vee dipole is designed and realized for use in pulse radiation applications, such as ground-penetrating radars. The resistive vee dipole is capable of radiating a broadband pulse whose shape is simply related to the input signal. In addition, it mostly eliminates the multiple reflections between the surface of the ground and the antenna because of its low radar cross section. Other investigators have studied the resistive vee dipoles using continuous loading. The antenna presented in this paper is printed on a circuit board and discretely loaded with off-the-shelf surface-mount chip resistors, making it easy, inexpensive to build, and mechanically stable. The characteristics of the antenna on a circuit board are measured and compared with the characteristics of the antenna in free space, which is numerically modeled using the method of moments code. The effects of the balun on the performance of the antenna are also presented.

Keywords: Resistive Vee Dipole, PCB, Wu-King profile

1. INTRODUCTION

A resistive vee dipole (RVD)[1–3] is a dipole bent at an angle with a resistive profile on the dipole arms. The resistive profile considered in this paper for the RVD is the Wu-King profile,[4] with which the current on a dipole arm travels away from the drive point without internal reflections. For practical antennas, the Wu-King profile may be approximated by an internal resistance per unit length:

$$R^i(r') = \frac{R_0}{1 - |r'/h|}, \quad R_0 = \frac{\eta_0 \Psi_0}{2\pi h} \tag{1}$$

where R_0 is the resistance per unit length at the drive point, r' is the distance along the arms from the drive point, η_0 is the wave impedance of free space, and h is the length of a dipole arm. For pulse radiation applications, the real parameter Ψ_0 is determined by trading off between the radiation efficiency and the amplitude of the tail ripples in the radiated waveform. RVDs with the Wu-King profile has many advantages inherited from its geometry and loading profile. It is geometrically simple and directive, and it operates over a broad bandwidth with a low radar cross section. It is also known to have the ability to radiate a broadband pulse whose shape is simply related to the input signal.

Various methods have been used to realize the Wu-King profile. One method involves depositing a resistive material of variable thickness on a dielectric rod.[5,6] With this method, one can build a cylindrical antenna for which the profile was developed, but it is difficult to achieve an accurate resistive profile. Another method to implement the profile is to taper a resistive film of constant thickness.[2,3] This method gives a better control over the resistive profile, but the realized structure is mechanically weak and the bonding between the resistive film and the metal at the drive point can be problematic. In a third method, one may use a series of discrete resistors that approximates the continuous profile. Maloney and Smith successfully approximated a resistive profile by stacking special high-frequency resistors in series.[7,8] However, this structure is mechanically fragile.

Further author information: (Send correspondence to K. Kim)
K. Kim: E-mail: gt6354a@mail.gatech.edu, Telephone: 1 404 894 3123
W. R. Scott: E-mail: waymond.scott@ece.gatech.edu, Telephone: 1 404 894 3048

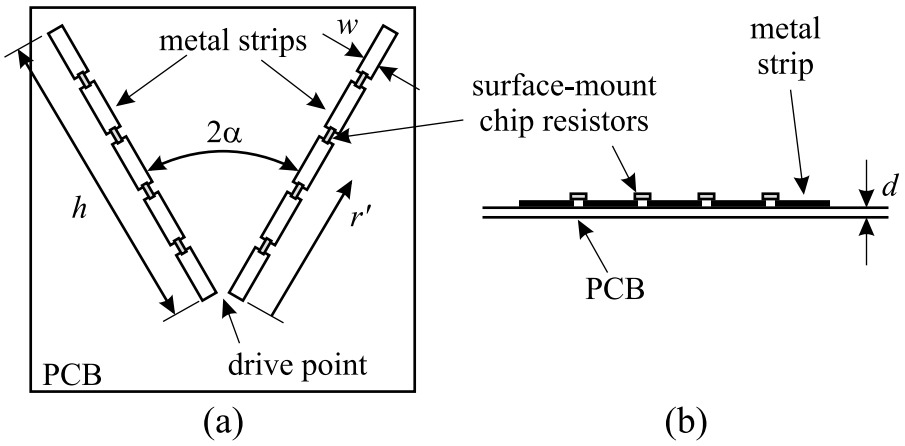

Figure 1. Diagram of an RVD printed on a circuit board. (a) Top view. (b) Side view.

As an alternative method to realize the resistive profile, we use standard off-the-shelf surface-mount chip resistors. The resistors are mounted on metal strips printed on a dielectric substrate using standard printed circuit board manufacturing technology. The structure is schematically drawn in Fig. 1. The resulting profile is accurate, easy to build, and mechanically stable. For the design of the RVD, the impedance per unit length at the drive point is chosen to be $R_0 = 1526\Omega/m$, and the length of a dipole arm is chosen to be $h = 30.6cm$. The remaining parameters are discussed in the next sections.

2. WU-KING PROFILE DISCRETIZATION

To realize the resistive profile with standard chip resistors, Eq. (1) is discretized. The arm of length h is divided into a number of sections, and a chip resistor is placed in the center of each section so that the resistance of the section agrees closely with that of Eq. (1). The chip resistors in this paper are 1.6mm in length. Thus, a maximum of 191 resistors can be used along each arm. However, to reduce the complexity and cost of the RVD, we will minimize the number of resistors used.

To investigate the number of resistors, three sets of resistors are used to discretize the continuous Wu-King profile. The RVDs with the discretized profiles are numerically modeled using the method of moments code in the electromagnetic interactions generalized (EIGER) code suite.[9] In the model, lumped resistor elements are used to simulate the chip resistors. The numerical model is used to predict the reflected voltage in the transmission line and the radiated field of the RVDs.

Fig. 2 shows the results from the numerical model when the input to the antenna is a Gaussian voltage pulse with $t_{FWHM}/\tau_a = 0.15$ incident in a 100Ω transmission line. Here, $\tau_a = h/c$ is the time required by light to travel the length of a dipole arm, and t_{FWHM} is the full-width half-maximum of the Gaussian pulse, which is expressed as

$$V(t) = V_0 e^{-\ln 16(t/t_{FWHM})^2}, \tag{2}$$

where V_0 is the maximum amplitude of the pulse. In Fig. 2, the graphs in the left column show the reflected voltages in the transmission line as functions of time, and the graphs in the right column show the radiated fields on boresight of the RVDs as functions of retarded time, $t_r = t - r/c$, where r is the observation distance.

In the graphs, the waveforms for the RVDs with 26 and 47 resistors for each arm look clean and simple; however, the waveforms for 11 resistors for each arm have ripples at the tails. Thus, the resistive profile discretized by 11 resistors poorly approximates the continuous profile, which is well approximated by 26 and 47 resistors. Because we want to minimize the number of resistors, we choose the discretization using 26 resistors. Fig. 3 shows the Wu-King profile discretized with 26 chip resistors. In the figure, the Wu-King profile is graphed in normalized conductance as a function of normalized distance, r/h. The discrete profile is plotted by dots at the locations of the chip resistors.

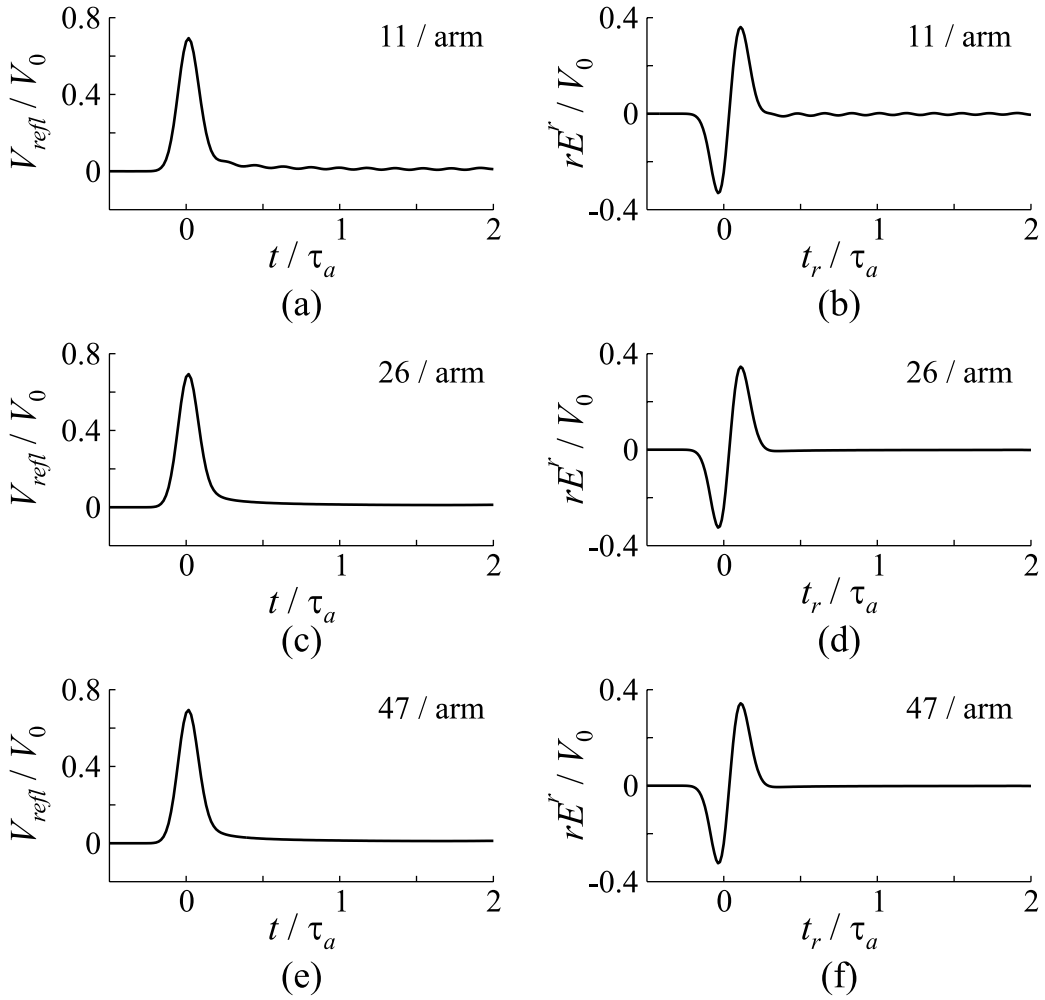

Figure 2. Waveforms predicted by the numerical model for the RVDs loaded with discrete profiles. The discrete profiles are obtained using (a), (b) 11 resistors, (c), (d) 26 resistors, and (e), (f) 47 resistors. The graphs in the left column are the reflected voltages in a 100Ω transmission line as functions of time, and the graphs in the right column are the radiated fields on boresight of the RVDs as functions of retarded time. The input signal for these graphs is a Gaussian voltage pulse incident in the 100Ω transmission line. The interior angle for the antennas is $2\alpha = 60^\circ$.

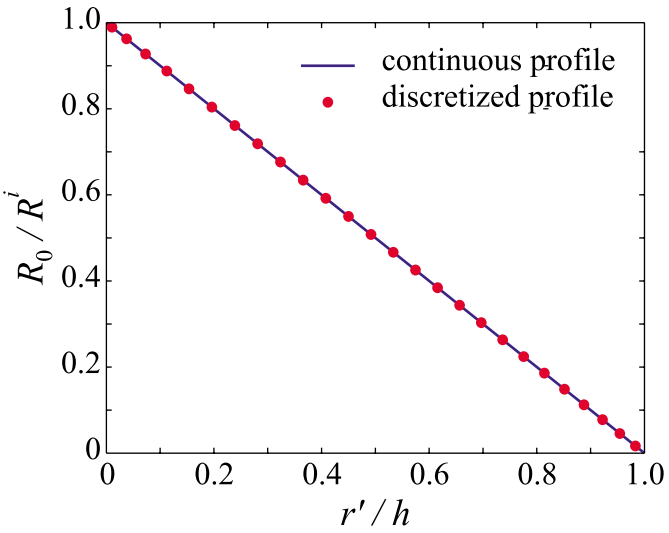

Figure 3. Wu-King profile. The continuous profile represented by normalized conductance is graphed as a function of normalized distance from the drive point. The discrete profile is plotted by dots at the locations of the chip resistors.

3. SUBSTRATE PROPERTIES

The substrate thickness also affects the performance of the antenna. To investigate the effects of the substrate thickness, the radiated field of the RVD is obtained from the numerical model for a number of substrate thicknesses*. Fig. 4 shows the radiated fields on boresight of the RVDs as functions of time when the antennas are excited by a Gaussian voltage pulse with $t_{FWHM}/\tau_a = 0.15$ incident in a 100Ω transmission line. Note that, in Fig. 4, the radiated waveforms as well as their amplitudes depend on the substrate thickness. The waveform is degraded with increasing substrate thickness. The reason for this is that the speed of current propagation on the antenna varies as a function of substrate thickness.

To investigate the effect of the substrate thickness on the speed of current propagation, the currents on the arms are obtained from the numerical model. In Fig. 5, the currents of an RVD without a substrate and the currents of an RVD with 1.6mm-thick FR-4 substrate are compared at 11 points along the arm. The currents are plotted as functions of time and vertically displaced according to the distance from the drive point when the antennas are excited by a Gaussian voltage pulse with $t_{FWHM}/\tau_a = 0.15$ incident in a 100Ω transmission line. As the current pulses travel away, the current pulse of the RVD with 1.6mm-thick FR-4 substrate appears later in time than that of the RVD without a substrate. Thus, the existence of the substrate slows down the speed of current propagation.

The effect of the substrate thickness and other geometrical factors on the radiated fields may be investigated using the numerical model. However, it is inconvenient to run the numerical model for a large number of cases. Thus, a simple analytical model is developed to investigate the relation between the geometrical factors and the radiated field of the RVD. To develop the analytical model, first note that the speed of current propagation, v, can be related to the medium surrounding the current as

$$v = \frac{c}{\sqrt{\epsilon_{re}}}, \tag{3}$$

where ϵ_{re} is the effective relative permittivity of the surrounding medium. The effective relative permittivity can be obtained by noting that the wavefront propagates approximately spherically for a wave launched at the

*EIGER cannot efficiently calculate the currents of the RVD on a finite sized substrate. They can be approximately obtained by using an infinite dielectric slab whose thickness is equal to the substrate. However, the radiated fields from the RVD on the slab are dispersed due to the infinite extent of the slab. This problem can be alleviated by first obtaining the currents on the dielectric slab, and then calculating the radiated fields from those currents when they are placed in free space instead of on the slab.

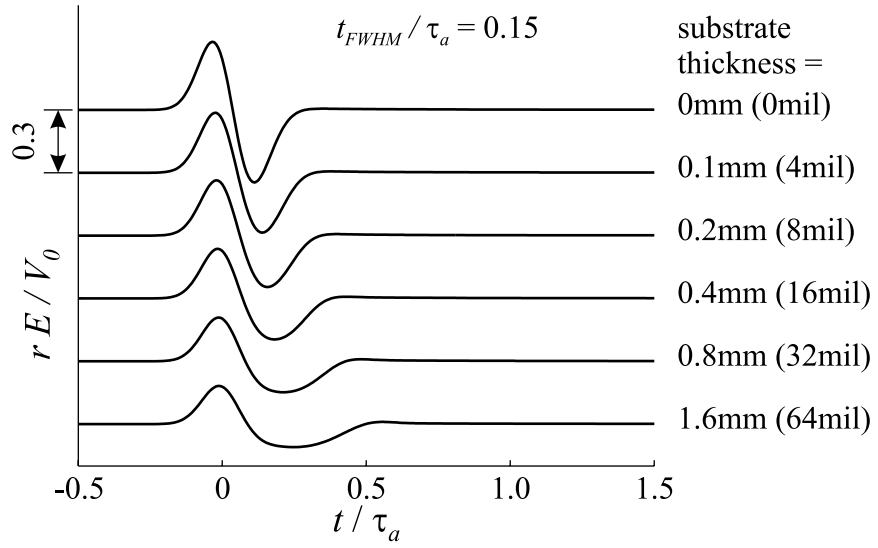

Figure 4. Normalized Radiated fields as functions of time for a Gaussian pulse with $t_{FWHM}/\tau_a = 0.15$ incident in a 100Ω transmission line. Each line represents the radiated field on boresight of an RVD with $2\alpha = 60°$ printed on an FR-4 substrate ($\epsilon_r = 4.2$) whose thickness varies from 0 to 1.6mm.

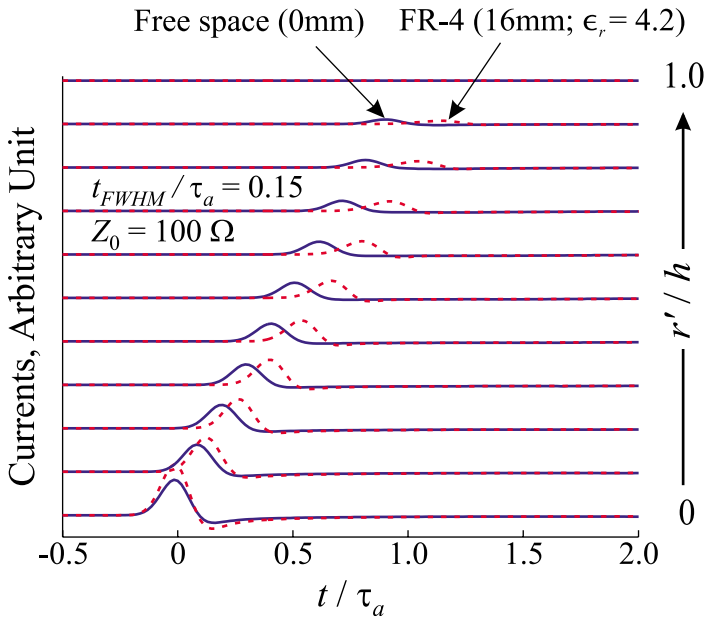

Figure 5. Comparison of currents at a number of points along the arms of the RVD without a substrate and the RVD with a 1.6mm-thick FR-4 ($\epsilon_r = 4.2$) substrate when a Gaussian pulse with $t_{FWHM}/\tau_a = 0.15$ is incident through a 100Ω transmission line. The interior angle of the antennas is $2\alpha = 60°$.

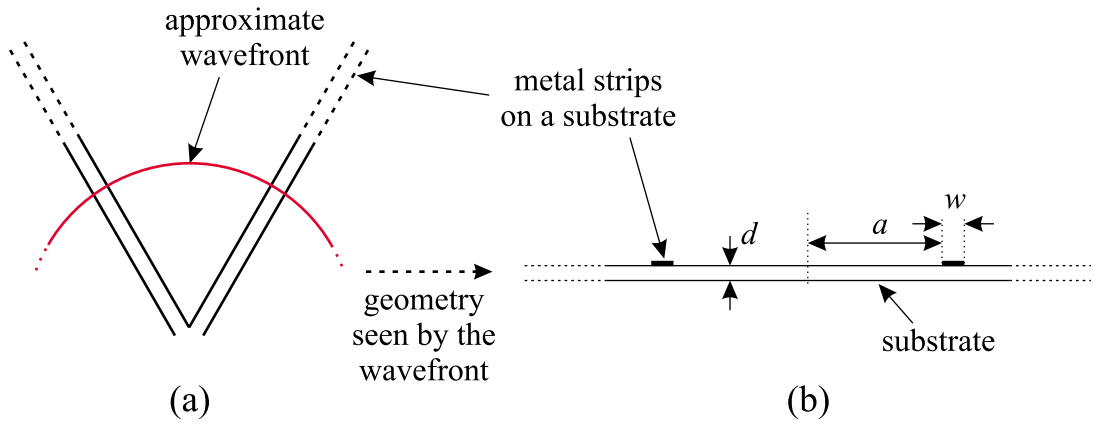

Figure 6. Diagrams of (a) the approximate wavefront propagating outwardly from the drive point and (b) the coplanar strip geometry seen by the wavefront.

drive point (Fig. 6). For this wavefront, the geometry of the RVD looks approximately like a pair of coplanar strips. Thus, the formulas developed for the coplanar strip geometry can be utilized to estimate ϵ_{re}:

$$\begin{aligned} k_1 &= a/(a+w), \\ k_2 &= \sinh\left(\frac{\pi a}{2d}\right) \Big/ \sinh\left(\frac{\pi(a+w)}{2d}\right), \\ \epsilon_{re} &= 1 + \frac{\epsilon_r - 1}{2} \frac{K(k_2^2)K(1-k_1^2)}{K(k_1^2)K(1-k_2^2)}, \end{aligned} \tag{4}$$

where a is the distance from the symmetry plane to the inner edge of the strip line, w is the width of the metal strip, d is the thickness of the substrate, and K is the complete elliptic integral of the first kind.[10, 11]

Fig. 7 shows the effective relative permittivity obtained using Eq. (4) for a RVD with $2\alpha = 44°$ on a substrate with $\epsilon_r = 3.4$. The effective relative permittivity is plotted as a function of substrate thickness for a number of metal strip widths. For the graph, the parameter a is obtained by first drawing a circle of radius $h/10$ centered at the drive point of the RVD and then taking the arc length from the symmetry plane to the inner edge of the metal strip. The figure shows that the effective relative permittivity decreases with decreasing substrate thickness for a fixed metal strip width. It also decreases with increasing metal strip width for a fixed substrate thickness.

The radiated fields of the RVD can be obtained by approximating the geometry into insulated thin wires and by using ϵ_{re} calculated above as the effective relative permittivity of the insulation. In an insulated thin wire loaded with the Wu-King profile, the current distribution may be approximated as[12]

$$I(r',t) = \pm I_0(t - r'/v)(1 - r'/h)[u(r') - u(r'-h)], \tag{5}$$

where $I_0(t)$ is the current at the drive point, $u(r')$ is the Heaviside unit step function, and r' is the distance from the drive point. The positive and negative signs are for the arms at angles α and $-\alpha$, respectively. Assume that v remains constant along the arm, and the current radiates in free space. Then, the radiated electric field in the plane of the RVD resulting from the current distribution is found to be

$$\begin{aligned} \bar{E}^r(\bar{r},t) = \hat{\theta}\frac{\mu_0 c}{4\pi r} \Bigg\{ & \left[\frac{\sin(\theta-\alpha)}{\sqrt{\epsilon_{re}} - \cos(\theta-\alpha)} - \frac{\sin(\theta+\alpha)}{\sqrt{\epsilon_{re}} - \cos(\theta+\alpha)} \right] I_0\left(t - \frac{r}{c}\right) \\ & - \frac{\sin(\theta-\alpha)}{h\left[\sqrt{\epsilon_{re}} - \cos(\theta-\alpha)\right]} \int_{r'=0}^{h} I_0\left(t - \frac{r}{c} - \frac{r'}{c}\left[\sqrt{\epsilon_{re}} - \cos(\theta-\alpha)\right]\right) dr' \\ & + \frac{\sin(\theta+\alpha)}{h\left[\sqrt{\epsilon_{re}} - \cos(\theta+\alpha)\right]} \int_{r'=0}^{h} I_0\left(t - \frac{r}{c} - \frac{r'}{c}\left[\sqrt{\epsilon_{re}} - \cos(\theta+\alpha)\right]\right) dr' \Bigg\}. \end{aligned} \tag{6}$$

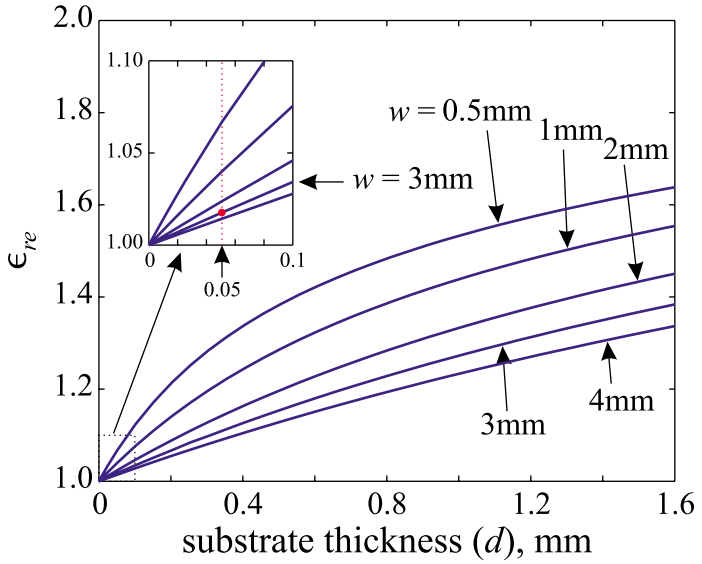

Figure 7. Effective relative permittivity experienced by an RVD with $2\alpha = 44^\circ$ on a substrate with $\epsilon_r = 3.4$ as a function of substrate thickness for a number of printed metal strip widths.

Using Eq. (4) and Eq. (6), the peak-to-peak amplitude of the radiated field on boresight ($\theta = 0$) of the RVD is plotted as a function of substrate thickness for a number of metal strip widths in Fig. 8 when the antenna is excited by a Gaussian current pulse with $t_{FWHM}/\tau_a = 0.15$ at the drive point. The peak-to-peak amplitude increases with decreasing substrate thickness for a fixed metal strip width. It also increases with increasing metal strip width for a fixed substrate thickness.

To investigate the relation between ϵ_{re} and the radiation pattern of the radiated field from the RVD, Eq. (6) is used to calculate the radiated electric fields of RVDs for a number of ϵ_{re}'s. Fig. 9 shows the peak-to-peak

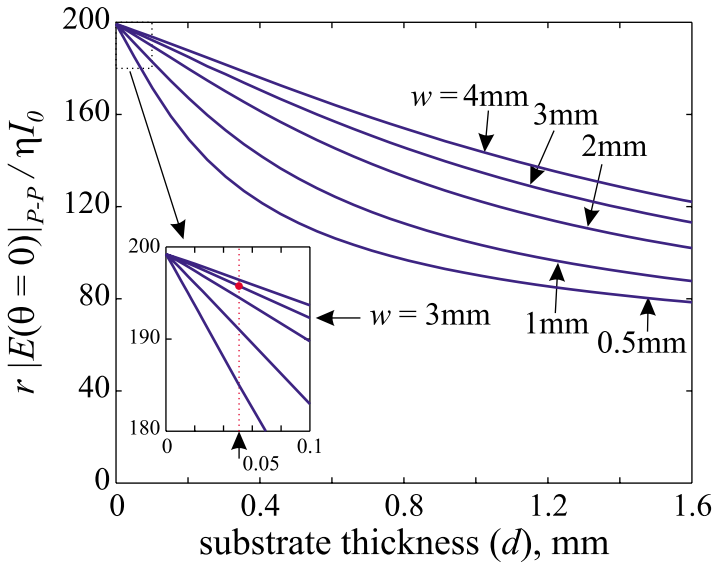

Figure 8. Normalized peak-to-peak amplitudes of the radiated electric fields on boresight of an RVD with $2\alpha = 44^\circ$ as functions of substrate thickness for a number of metal strip widths. The simple analytical model is used to calculate the amplitudes. The antenna is excited by a Gaussian current pulse with $t_{FWHM}/\tau_a = 0.15$ at the drive point.

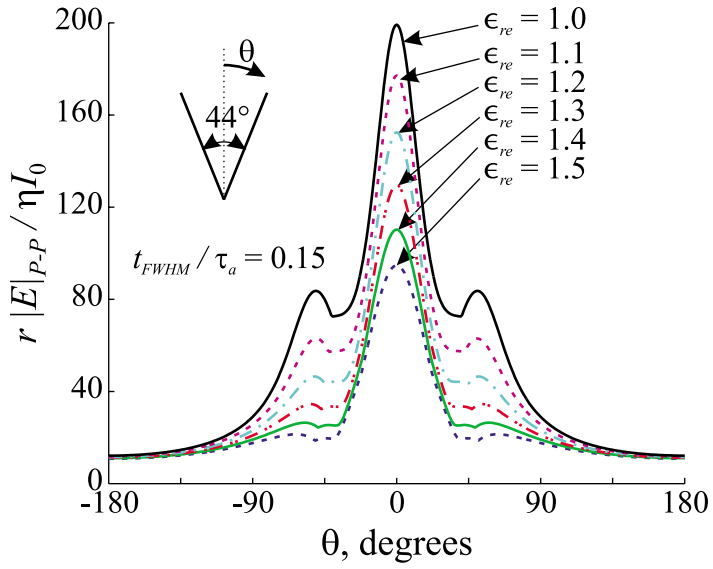

Figure 9. Comparison of the peak-to-peak amplitudes of the radiated electric fields of RVDs with $2\alpha = 44°$ over a range of ϵ_{re}. The relative permittivity of the substrate is $\epsilon_r = 3.4$. The source current $I_0(t)$ is a Gaussian pulse with $t_{FWHM}/\tau_a = 0.15$. The simple analytical model developed is used to calculate the amplitudes.

amplitude of the radiated electric field ($|E|_{P-P}$) normalized by $\eta I_0/r$ as a function of observation angle when the antenna is excited by a Gaussian current pulse with $t_{FWHM}/\tau_a = 0.15$ at the drive point. Note that the amplitude at angles such that $|\theta| < 90°$ strongly depends on ϵ_{re}. The amplitude at $\theta = 0$ drops about 10% for each 0.1 increment of ϵ_{re}. However, at $|\theta| > 90°$, the amplitudes do not vary much.

To decrease ϵ_{re} or to increase the peak-to-peak amplitude, one has to use a thin substrate with a small ϵ_r and have wide metal strips. However, note that the metal strip width must be chosen such that it is comparable with the width of chip resistors.

4. EXPERIMENTAL RESULTS

A resistive vee dipole has been designed and realized based on the discussions in the previous sections. The interior angle has been chosen to be 44°, the substrate has been chosen to be a 0.05mm-thick Kapton® ($\epsilon_r = 3.4$),[13] and the metal strip width has been chosen to be 3mm.[14] For this design, ϵ_{re} is about 1.015 at $r'/h = 0.1$ as marked by a dot in Fig. 7. The peak-to-peak amplitude of the RVD with ϵ_{re} is marked by a dot in Fig. 8, which along with Fig. 9 shows a reduction of less than 1.5% from the peak-to-peak amplitude of the RVD without a substrate.

Fig. 10 (a) shows the realized RVD. The arms are printed 3mm wide on a Vee-shape 0.05mm-thick Kapton® substrate with interior angle 44°. Each arm is loaded with 26 surface-mount chip resistors. Because the 0.05mm-thick Kapton substrate is thin and fragile, it is attached to a thick blank FR-4 substrate to enhance the mechanical strength. The picture of the FR-4 substrate is shown in Fig. 10 (b). The FR-4 substrate is carved out underneath the RVD.

To see the performance of the realized RVD, the reflected voltage in the transmission line and the radiated fields at a number of observation angles have been measured. Fig. 11 shows the reflected voltage in a 100Ω transmission line as a function of time for a Gaussian voltage pulse with $t_{FWHM}/\tau_a = 0.15$ incident in the transmission line. The figure compares the voltage obtained from the measurement with the voltage obtained from the numerical model in which the RVD does not have a substrate. The agreement is good, and therefore the realized RVD works well in terms of the reflected voltage.

The radiated fields are measured by a small dipole probe shown in Fig. 12, which is placed at an angle in the plane of the RVD at $r = 2.72$m away from the drive point of the RVD. The dipole probe is 4cm long and

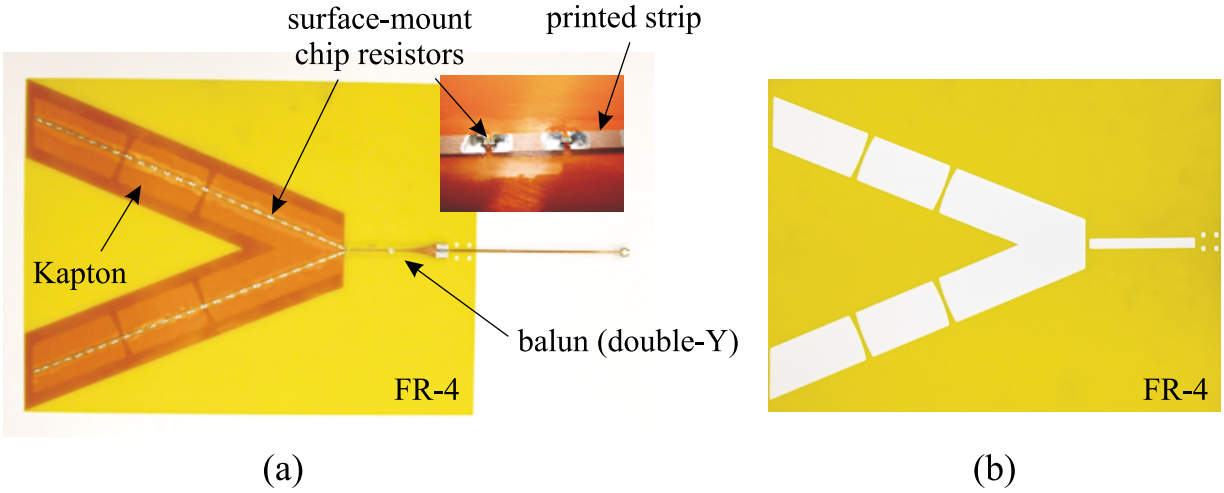

Figure 10. Realized RVD. (a) Picture of realized RVD. The RVD is printed on a vee-shape Kapton film, which is attached to a thick FR-4 substrate to enhance the mechanical strength. In this figure, the RVD is fed by a double-Y balun. (b) Picture of the FR-4 substrate. The substrate is carved out underneath the RVD.

connected to a 100Ω balanced transmission line. In Fig. 13, the voltage (V_L) across the dipole probe is plotted as a function of time and vertically displaced according to the angular location of the dipole probe. The solid lines represent the results from the numerical model where the RVD does not have a substrate, and the dotted lines represent the results from the measurement. The agreement is good, and therefore the realized RVD works well in terms of the radiated field. The amplitudes of the radiated fields are slightly higher. This is believed to be from a small error in the calibration procedure.

Because the RVD has a symmetrical geometry, a balun structure is required. Two balun structures have been tested for use with the RVD. The RVDs with identical baluns are placed $r = 2.72$m apart facing each other (Fig. 14 (a)), and the voltage at the balun input is measured. Fig. 15 compares the measured results with the numerical results. In the numerical model, the RVDs have ideal baluns.

Fig. 15 (a) shows the results with a balun assembly whose schematic is shown in Fig. 14 (b). The balun assembly is made using a Picosecond Pulse Labs Model 5315A Balun[15] and a pair of 60cm-long 50Ω semi-rigid coaxial cables. The coaxial cables are connected to the two output ports of the balun, which are 180° different in phase. The outer conductors of these cables are connected together forming a 100Ω balanced transmission line. The 60cm-long cable pair provide a time window of about 5.8nsec in which no multiple reflections exist

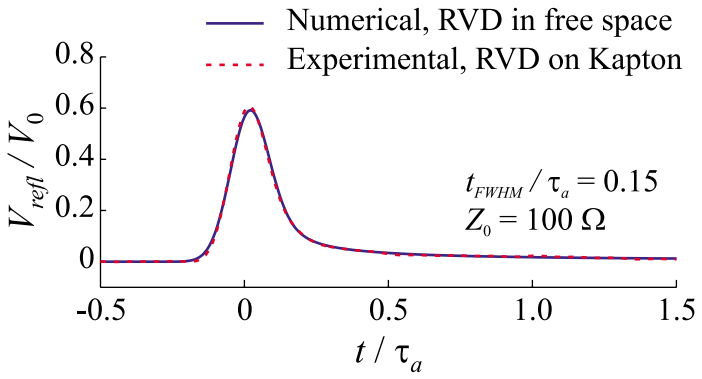

Figure 11. Comparison of reflected voltages in the 100Ω-feeding transmission line as functions of time for a Gaussian pulse with $t_{FWHM}/\tau_a = 0.15$.

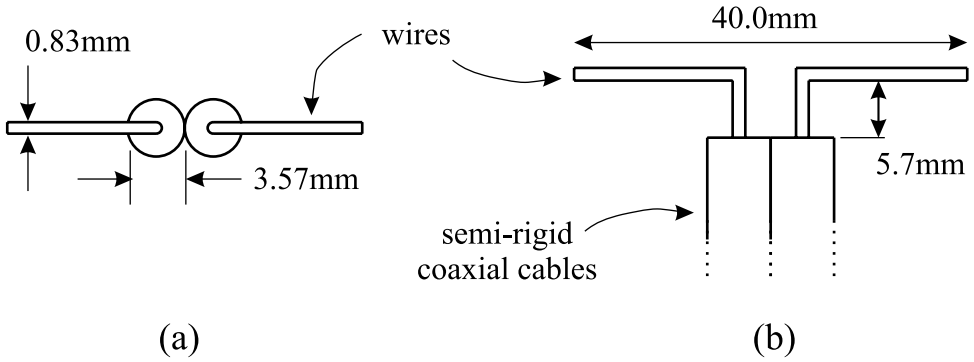

Figure 12. Dimension of the dipole probe. (a) Top view. (b) Side view. The dipole arms are essentially the extensions of the center conductors of the semi-rigid coaxial cables. Below the dipole, two semi-rigid coaxial cables form a 100Ω-balanced transmission line.

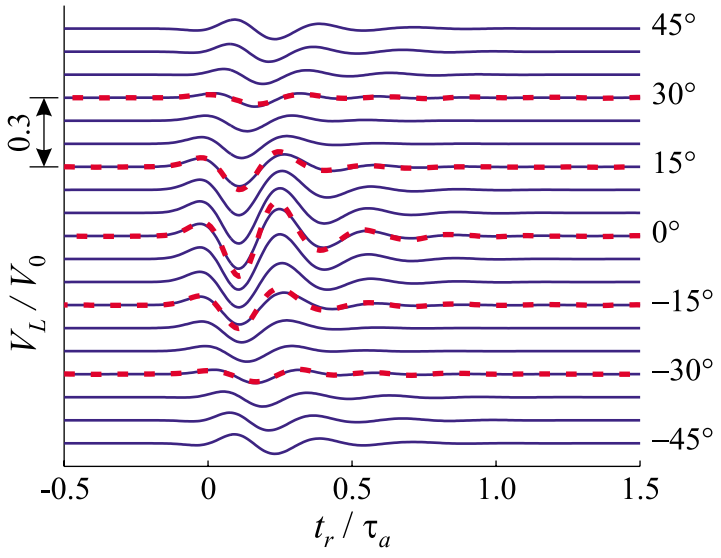

Figure 13. Voltages in a 100Ω transmission line connected to a dipole probe. The dipole probe is 2.72m away from the RVD at an angle. The input pulse to the RVDs is a Gaussian pulse with $t_{FWHM}/\tau_a = 0.15$ through the 100Ω transmission line.

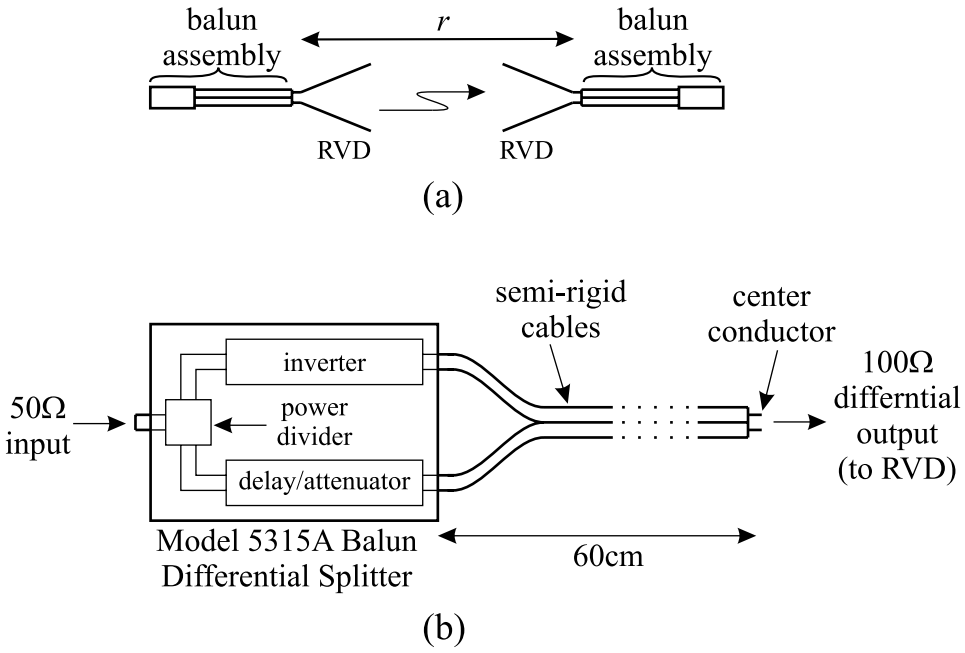

Figure 14. Boresight radiation measurement with balun assembly. (a) boresight radiation measurement (r = 2.7m). (b) balun assembly.

between the antenna and the balun. Fig. 15 (b) shows the results with double-Y baluns[16] with characteristic impedance $Z_0 = 188\Omega$. The graphs show that the RVD works well with the double-Y balun. The measured amplitude is lower than the ideal case due to the balun insertion loss. A bump seen at $t_r/\tau_a \simeq 0.6$ is believed to be from a reflection inside the balun.

5. CONCLUSION

A practical way to build a RVD was proposed and discussed. A RVD was realized on a PCB according to the discussion. The performance of the realized RVD was investigated through experiments. The results show that the performance of the RVD on the PCB was as good as the RVD without a substrate. The realized RVD was tested with two types of baluns. The test showed that the RVD works well with a double-Y balun.

ACKNOWLEDGMENTS

This work is supported in part by the US Army Night Vision Electronic Systems Directorate, Countermine Division.

REFERENCES

1. T. P. Montoya and G. S. Smith, "Resistively-loaded vee antennas for short-pulse ground penetrating radar," in *IEEE Int. Antennas Propagat. Symp. Dig.*, pp. 2068–2071, Jul. 1996.
2. T. P. Montoya, *Vee Dipole Antennas for Use in Short-Pulse Ground-Penetrating Radars.* PhD thesis, Georgia Institute of Technology, Mar. 1998.
3. T. P. Montoya and G. S. Smith, "Land mine detection using a ground-penetrating radar based on resistively loaded vee dipoles," *IEEE Trans. Antennas Propagat.* **47**(12), pp. 1795–1806, Dec. 1999.
4. T. T. Wu and R. W. P. King, "The cylindrical antenna with nonreflecting resistive loading," *IEEE Trans. Antennas Propagat.* **AP-13**(3), pp. 369–373, May 1965. Correction, p. 998, Nov. 1965.
5. L. Shen, "An experimental study of the antenna with nonreflecting resistive loading," *IEEE Trans. Antennas Propagat.* **AP-15**(5), pp. 606–611, Sep. 1967.

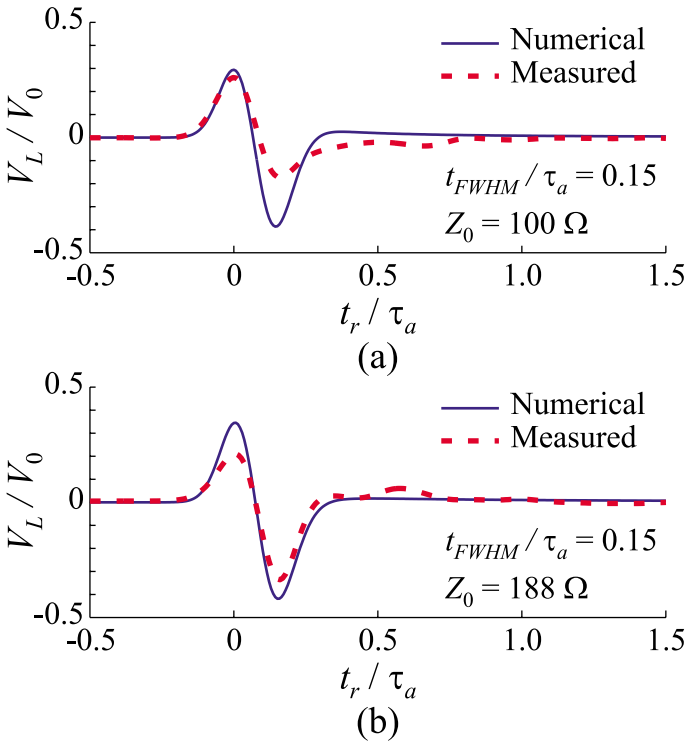

Figure 15. Results from the face-to-face measurements. The solid lines represent the numerical results, where the RVDs do not have a substrate and are connected to ideal baluns. The dotted lines represent the measured results. The baluns used for the measurement are (a) a balun assembly and (b) double-Y baluns.

6. J. F. Lally and D. T. Rouch, "Experimental investigation of the broad-band properties of a continously loaded resistive monopole," *IEEE Trans. Antennas Propagat.* **AP-18**(6), pp. 764–768, Nov. 1970.
7. J. G. Maloney, *Analysis and Symthesis of Transient Antennas using the Finite-Difference Time-Domain (FDTD) Method*. PhD thesis, Georgia Institute of Technology, Nov. 1992.
8. J. G. Maloney and G. S. Smith, "A study of transient radiation from the Wu-King resistive monopole - FDTD analysis and experimental measurements," *IEEE Trans. Antennas Propagat.* **41**(5), pp. 668–676, May 1993. Correction, vol. 43, no. 2, p. 226, Feb. 1995.
9. R. M. Sharpe, J. B. Grant, N. J. Champagne, W. A. Johnson, R. E. Jorgenson, D. R. Wilton, W. J. Brown, and J. W. Rockway, "EIGER: Electromagnetic interactions generalized," in *IEEE AP-S Int'l Symp. Digest, Quebec, Canada*, pp. 2366–2369, Jul. 1997.
10. M. Abramowitz and I. A. Stegun, *Handbook of Mathematical Functions with Formulas, Graphs, and Mathematical Tables*, New York: Dover, 1972.
11. K. C. Gupta, R. Garg, I. Bahl, and P. Bhartia, *Microstrip Lines and Slotlines*, Artech House, 2 ed., 1996.
12. G. S. Smith, *An Introduction to Classical Electromagnetic Radiation*, ch. 4. Cambridge, UK: Cambridge University Press, 1997.
13. E.I. du Pont de Nemours and Company (2003, Mar. 7), "DuPont Kapton® Polymide Film." [Online]. Avaliable: http://www.dupont.com/kapton/.
14. K. Kim, *Numerical and Experimental Investigation of Impulse-Radiating Antennas for Use in Sensing Applications*. PhD thesis, Georgia Institute of Technology, April 2003.
15. Picosecond Pulse Labs (2001, May 5), "Model 5315A Balun, Differential Pulse Splitter Specification Sheet." [Online]. Avaliable: http://www.picosecond.com.
16. J. B. Venkatesan and W. R. Scott, Jr., "Investigation of the double-Y balun for feeding pulsed antennas," in *SPIE Aerosense*, 2003.